Proceedings of the 2007 American Control Conference
Marriott Marquis Hotel at Times Square
New York City, USA, July 11-13, 2007

WeA14.3

Modeling and Optimization Analysis of Single Flagellum Bacterial Motion

Edgar Lobaton[1] and Alexandre Bayen[2]

Abstract— Bacteria such as *Rhodobacter sphaeroides* use a single flagellum for propulsion and change of orientation. Simple organisms such as this have inspired nanorobotic designs with potential applications in medicine which motivates the present work. In this article, an elastic model for a single flagellum bacterium is presented and followed by an analysis of the system based on optimization. The model is based on the method of Regularized Stokeslet which allows for a discretization of the system into particles which are connected by spring forces. An optimal elasticity distribution that maximizes the mean forward speed is obtained. These elasticity coefficients are obtained through the use of an adjoint-based optimization scheme. The results are illustrated through a simulation showing improvement on the swimming patter of the bacteria.

I. INTRODUCTION

A bacterial flagellum is a helical structure attached to the body of bacteria which is used for locomotion. A mechanism that drives the motion of bacteria is chemotaxis. Several studies explain the patterns observed in bacteria due to this mechanism. In particular, J. P. Armitage and R. Schmitt [1] describe the type of swimming patterns observed in different bacteria that use flagella for their locomotion. *Rhodobacter sphaeroides* is a particular example of such bacteria which uses a single flagellum for motion.

Bacteria have a motor at the base of each flagellum which applies a rotational torque. This torque forces the base of the flagellum to rotate and the rest of the structure moves due to the elastic forces joining it together, i.e. there are no internal forces generated in the flagellum just reactive forces due to stretching. When the direction of the torque agrees with the handedness of the flagellum, the bacteria moves forward while the flagellum stretches. If the torque is turned off, the flagellum returns to its original position. It is stated in a paper by J. P. Armitage et al. [2] that bacteria such as *Rhodobacter sphaeroides* change direction just by stopping rotation, while other bacteria such as *Escherichia coli* reorient themselves by switching the direction of their torques. Figure 1 shows the flagellar conformations of *R. sphaeroides* at different stages of the motion process. In figure 2 it is observed that the simulated model also demonstrates similar conformations.

Analysis on the propulsion mechanism of a single flagellum has been done before by researchers such as E. Purcell [3]. However, this type of analysis often ignores the dynamics of the system, any elasticity considerations, and neglects the
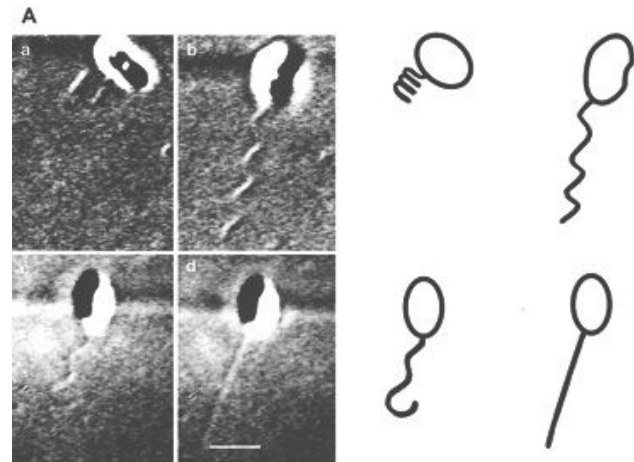
[1]Ph.D. student, Electrical Engineering and Computer Science Dept., University of California-Berkeley, lobaton@eecs.berkeley.edu

[2]Assistant Professor, Dept. of Civil and Environmental Engineering, University of California-Berkeley, bayen@berkeley.edu

Fig. 1. Flagellar conformations in *R. sphaeroides* from the article [2] by J. P. Armitage et al. Bar represents 1 μm.

effect of the body. On the other hand, simulation studies such as the one performed by H. Flores et al. [4] include the dynamics of the system and elasticity on the flagellum. However, the model in [4] does not include the effect of the bacterial body.
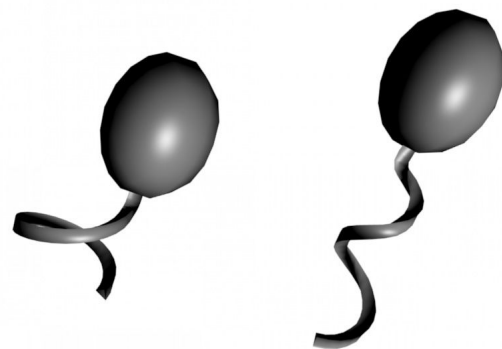

Fig. 2. Modeled Bacteria in its rest position (left) and during motion (right).

The recent years have stressed an increased interest in developing models of swimmers at low-Reynolds number. The interest ranges from biological to nanotechnology applications. For example, a model that uses three spheres for motion was introduced by A. Najafi and R. Golestanian [5]. R. Dreyfus et al. [6] built a microscopic artificial swimmer with a flagellum composed of a chain of colloidal magnetic particles linked by DNA. At a macro scale, J. Long et al.

[7] build a simple robot that demonstrates the dynamics underlying helical trajectory on microscopic organisms. Also B. Behkam at al. [8] perform a propulsion analysis of a single flagellum in a silicone oil tank.

In this article, the model presented by H. Flores et al. [4] is expanded to model and analyze bacteria with a single flagellum such as *R. sphaeroides*. This model includes a bacterial body and an "engine" that drives the rotation of the structure. The motion for the model is studied, and some key observations on the trajectory of the structure are highlighted. The model uses a combination of closed form solutions of *Stokes' equations*: the *regularized Stokeslet* and *rotlet*. The model is analyzed: we investigate the influence of the elasticity distribution in the flagellum of the bacteria on the forward thrust motion. In particular, we characterize an optimum value of the elasticity which provides maximal thrust. This type of analysis can be used for systems biology parameter estimation [9], [10], as well as for design, in particular for micromachines [6], [8], which is a motivation for this work.

We pose the problem as an optimization program, in which the underlying flow of the problem (governed by Stokes' equations) appears in the constraints. We solve this problem with adjoint-based optimization. The specificity of the method proposed in this article lies in the use of the closed form *regularized Stokeslet* and *rotlet* solutions in the computation of the full solution of the direct and the adjoint problems. Adjoint-based control or optimization has proved to be a very efficient technique for shape optimization [11], flow control [12], [13], parameter estimation in biology [9], control of networks [14], [15]. In most of adjoint work available in the literature, the gradient of the cost function of the optimization problem is computed explicitly in terms of the solution of the adjoint and the direct problems; note that, the actual numerical solution of the problem has to rely on numerical schemes to solve the corresponding PDEs. In the present work, the specific structure of the system enables us to write the gradient explicitly in term of the closed form solutions of Stokes' equation, which provides an enormous gain in computational efficiency and numerical accuracy.

This article is organized as follows: first, the model is introduced by reviewing the scheme used for discretization of the structure and displaying some motion results; then, the adjoint-based optimization analysis is presented by showing the derivations and discussing the implications of our results.

II. MODELING

The model consists of the bacterial body, a helical flagellum, and the junction connecting them. The junction, which consists of a hook coming out of the bacterial body and attached to the helical flagellum, has at its base the rotor engine that drives the motion. In section II-B the engine is modeled by a set of torques. These torques are the active components that drive the motion of the whole structure. The flagellum is a helical-shaped elastic structure that moves due to the forces and torque effects that are imposed on it. Of course, all of these interactions must be computed in an

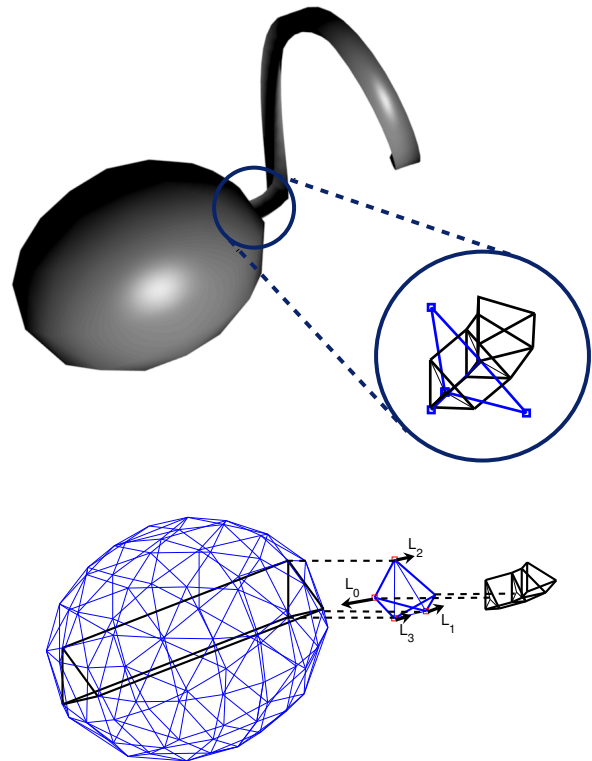environment of low-Reynolds number which characterizes the scale of the organism to be modeled.

Fig. 3. Rotor and junction structures shown together (top) and as separate components (bottom).

The bacterial structure is discretized into a set of particles joined by a network of springs (see figure 3), which have forces and torques applied to them. The motion of these particles obey a set of PDEs as it is described in the next section.

A. The Particle Method

Due to the low-Reynolds number that characterizes this system, the hydrodynamics of the system can be properly described with the Stokes equations. These equations in dimensionless form are given by:

$$\begin{aligned} \Delta u &= \nabla P - f \\ \nabla u &= 0 \end{aligned} \quad (1)$$

where u is the fluid velocity, P is the fluid pressure, and f is the external force density.

Here we use the *regularized Stokeslet* and *regularized rotlet* solutions derived by H. Flores et al. [4] for the cases of a single point force f_0 and a single point torque L_0 applied at location x_0. The *regularized Stokeslet* solution is given by

$$U_s(x; x_0, f_0) = \frac{(r^2+2\delta^2)}{8\pi(r^2+\delta^2)^{3/2}} f_0 + \frac{[f_0^T(x-x_0)]}{8\pi(r^2+\delta^2)^{3/2}} (x - x_0),$$

$$(2)$$

and the *regularized rotlet* solution is given by

$$U_r(x; x_0, L_0) = \frac{(2r^2 + 5\delta^2)}{16\pi(r^2 + \delta^2)^{5/2}} [L_0 \times (x - x_0)], \qquad (3)$$

where r is the distance between x and x_0, and δ is the regularizing parameter in the method. These formulas express analytical solutions to a regularized version of the Stokes equations (1) in which the forces and torques are not applied at single points, but are distributed over a small neighborhood of the application point. For more details refer to [4].

These closed form solutions give us a velocity field that can be used to track particles moving in the fluid. Hence, we only require a model that specifies the forces and torques due to a particular configuration at a specified time. In this model, the effect of the forces (which are defined at all particle locations) and the torques (applied at a total of 4 locations) can be combined to define the following dynamics for the system:

$$\dot{x}_k = \sum_{i=0}^{3} U_r(x_k; x_{n_i}, L_i) + \sum_{j=1}^{N_x} U_s(x_k; x_j, f_j) \qquad (4)$$

where $n_i \in R$, the set of indices where torques are applied, and N_x is the total number of particles. See figure 3 and section II-B for an illustration.

B. Bacterial Model

The bacterial model follows the same methodology developed by H. Flores et al. [4]. The flagellar structure and the body of the bacteria are discretized into a collection of particles with a network of springs connecting them. A view of some of these connections is shown in figure 3 and figure 4.

The particles and spring connections on the body of the bacteria (which is defined as an ellipsoid) define a triangular tessellation of its surface. Besides having spring connections on the surface of the body, we also define connections between the front and back particles in the body. These are marked with dark lines in the bottom-left plot of figure 3. These connections are there to make the structure more stable.

The flagellum is discretized by using triangular cross sections perpendicular to the helix that determines the centerline of the structure. The types of spring connections in the flagellum are cross sectional, longitudinal, diagonal, and anti-diagonal (see figure 4).
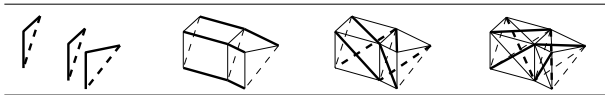

Fig. 4. Springs on the flagellum: Cross-sectional, longitudinal, diagonal, and anti-diagonal (from left to right).

The body is joined to the flagellum by a junction shaped as a hook. This junction is discretized in the same way as the flagellum. The junction is connected to the head through the rotor engine. This engine is discretized allowing for free

rotation of the junction. At the bottom of figure 3 the engine structure (which is a diamond-like structure joined to the body) and part of the junction are shown. The top of figure 3 shows these components together and their location in the bacterial model.

Forces due to the stretching of a spring are defined by using Hooke's law. The total force at a point x_i is the summation of the forces due to all the particles connected to it, and it is given by

$$f_j = \sum_{n \in c(j)} \alpha_{jn} \left(1 - \frac{r_{0,jn}}{r_{jn}} \right) (x_n - x_j), \qquad (5)$$

where $c(j)$ is the set of indexes of particles connected to x_j by spring, α_{jn} is the elasticity of the spring connection between x_j and x_n, r_{jn} is the distance between the particles, and $r_{0,jn}$ is the rest length of the corresponding spring.

The driving force in the engine are the torques. A main torque L_0 is applied at location x_{n_0}, and counter-torques L_i are applied at locations x_{n_i} for $i = 1 \ldots 3$. The location of the torques are shown at the bottom of figure 3. All of these torques are defined to be parallel. The magnitude σ_0 of the main torque is given by σ, and the magnitude σ_i of the counter-torques is given by $-\sigma/3$ which is chosen to conserve angular momentum. The equation of any of the torques is given by

$$L_i = \sigma_i \frac{p}{||p||}, \qquad (6)$$

where $p \triangleq (x_{n_0} - (x_{n_1} + x_{n_2} + x_{n_3})/3)$. The vector p points in the same direction as the tangent to the axis of rotation of the junction.
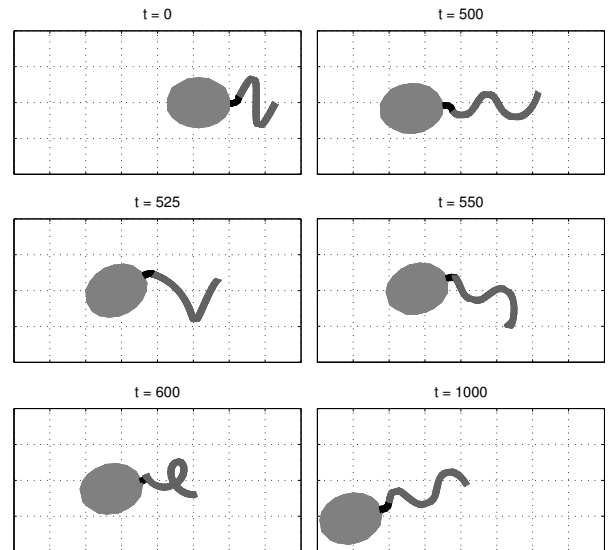
C. Motion Results

Fig. 5. Motion simulation illustrating a change of orientation due to reversing the torque at $t = 500$.

Figure 5 shows some plot at different stages of a simulation. For this simulation, the torque is turned-on at time

$t = 0$, its direction is reversed at time $t = 500$, and it is set again to its original magnitude at $t = 530$. Initially the flagellum has a small pitch (top-left). As the structure moves, the flagellum stretches (top-right). The structure changes orientation when the torque is reversed (middle-left), and reorients itself (middle-right) when the torque is reset. Finally, the structure moves in a new direction (bottom-right) with a change of orientation of about $30 \deg$.

Animation of the motion can be seen at:
http://www.ce.berkeley.edu/~bayen/acc07/acc07.html.

III. ADJOINT-BASED SPEED OPTIMIZATION

The goal of this section is to analyze the elasticity distribution over the flagellum. In particular, we show how to optimize average forward speed by varying the elasticity. Gradient ascent will be used to obtain the maximum of a functional that is specified below. The derivation of the gradient is performed using the adjoint problem since a direct computation would be computationally expensive.

A. Optimization Problem with PDE Constraints

The optimization problem is to find the optimal elasticity distribution over the flagellum that maximizes the mean forward speed of our structure given that the dynamics are constrained by the Stokes equations (1).

Due to the complex motion of the structure, the mean forward speed v is not a quantity that can be obtained in closed form. However, it can be approximated by considering the average distance traveled by a particle k, i.e.

$$v \approx \frac{1}{T}||x_k(T) - x_k(0)||_2.$$

This is a good approximation for large enough T. Hence, the following objective functional is defined from considering the distance traveled by the average among all particles:

$$J(\alpha) = \frac{1}{2}\left(\frac{||\bar{x}(T;\alpha) - \bar{x}(0;\alpha)||_2}{T}\right)^2 \quad (7)$$

where $\bar{x}(t;\alpha) = \sum_{i=1}^{N_x} x_i(t;\alpha)/N_x$, α encodes the design parameters (in our case, the elasticity distribution over the flagellum), and N_x is the number of particles in the structure. The dependency of the trajectories on α is emphasized by using the notation $x_i(t;\alpha)$. The average among all particles can be thought as a center of mass computation. The design parameter α only appears explicitly on the computation of the forces between particles as seen in section II-B. In turn, these forces specify the velocity flow field that updates the position of the particles.

Therefore, the optimization problem is posed as the maximization of the objective functional given in equation (7) with constraints given by equation (4), where the forces and torques are defined by the current configuration of the structure.

B. Considerations due to Periodic Configuration

Due to the physical nature of the motion, it is expected to find periodic behavior associated with the configuration of the structure. This is also observed from the numerical data. Hence, it can be assumed that the motion of a particle is of the form

$$x_k(t) = x_k(0) + vt\hat{e}_1 + p_1(t)\hat{e}_1 + p_2(t)\hat{e}_2 + p_3(t)\hat{e}_3, \quad (8)$$

where $p_i(t)$ are periodic functions of period τ and $p_i(0) = 0$, $\hat{e}_1$ is the unit vector in the direction of the mean velocity, and $\{\hat{e}_i\}$ form an orthonormal basis. This implies

$$\frac{1}{T^2}||\bar{x}(T) - \bar{x}(0)||_2^2 = v^2 + O\left(\frac{1}{T}\right).$$

Using this result and equation (7), then

$$J(\alpha) = \frac{1}{2}v^2 + O\left(\frac{1}{T}\right).$$

Note that if $T \triangleq N\tau$, where N is an integer and the motion is exactly periodic, then the last term vanishes. However, using this for the adjoint computation would require knowing τ analytically as a function of α. In order to reduce the last term in the functional evaluation, T is computed such that $T \approx N\tau$ by minimizing the L_2 difference between configurations after some fixed time.

From the previous equation, it also follows that

$$D_\alpha J(\alpha) = v^T(D_\alpha v) + O\left(\frac{1}{T}\right).$$

In this case, the last term does not vanish for $T = N\tau$, but it becomes a better estimate to $v^T(D_\alpha v)$ as $T \to \infty$. The later is of interest since the goal is to maximize the mean forward speed.

C. Adjoint Derivation

By perturbing the system and noting that the i-th elasticity coefficient α_i (here we are assuming an ordering of the coefficients) only appear explicitly in the computation of the forces, we have

$$
\begin{aligned}
\dot{x}'_k &= \sum_{i=0}^{3}(D_1 U_r(x_k; x_{n_i}, L_i)x'_k \\
&\quad +D_2 U_r(x_k; x_{n_i}, L_i)x'_{n_i} \\
&\quad +D_3 U_r(x_k; x_{n_i}, L_i)L'_i) \\
&\quad + \sum_{j=1}^{N_x}(D_1 U_s(x_k; x_j, f_j)x'_k \\
&\quad +D_2 U_s(x_k; x_j, f_j)x'_j \\
&\quad +D_3 U_s(x_k; x_j, f_j)f'_j) \\
L'_i &= \sum_{m \in R}(D_{x_m} L_i)x'_m \\
f'_j &= \sum_{m=1}^{N_x}(D_{x_m} f_j)x'_m + \sum_{n=1}^{N_\alpha}(D_{\alpha_n} f_j)\alpha'_n.
\end{aligned} \quad (9)
$$

where it is assumed that the first N_α elasticity coefficients are the ones used for the optimization, D_i stands for the gradient with respect to the i-th entry, and $\{x'_k, f'_k, L'_k\}$ are the corresponding first order variations.

By recombining all of these terms the above equation can be expressed as

$$
\begin{aligned}
\dot{x}'_k(t) &= \sum_{i=1}^{N_x} F_{k,i}(S(t))x'_i(t) \\
&\quad + \sum_{j=1}^{N_\alpha} G_{k,j}(S(t))\alpha'_j \\
x'_k(0) &= 0,
\end{aligned} \quad (10)
$$

where $S(t)$ stands for the configuration of the structure at time t. Definitions and explicit formulations of $F_{k,i}$, $G_{k,j}$ are given in Appendix I.

The first variation of the energy functional given in equation (7) is given by

$$J'(\alpha) = \frac{1}{N_x T^2} \sum_{i=1}^{N_x} (\bar{x}(T) - \bar{x}(0))^T x_i'(T). \qquad (11)$$

The adjoint state $y_k(t)$ is defined in order to obtain an analytical expression in terms of α_k'. Multiplying both sides of equation (10) by the transpose of the corresponding adjoint state and integrating over time, then

$$\int_0^T y_k^T(t)\dot{x}_k'(t)\,dt = y_k^T(T)x_k'(T) - \int_0^T \dot{y}_k^T(t)x_k'(t)\,dt$$
$$\int_0^T y_k^T(t)\dot{x}_k'(t)\,dt = \int_0^T y_k^T(t)\sum_{i=1}^{N_x} F_{k,i}(S(t))x_i'(t)\,dt$$
$$+ \int_0^T y_k^T(t)\sum_{j=1}^{N_\alpha} G_{k,j}(S(t))\alpha_j'\,dt.$$

By summing over all particles, then

$$\sum_{k=1}^{N_x} y_k^T(T)x_k'(T) = \sum_{i=1}^{N_x} \int_0^T \dot{y}_i^T(t)x_i'(t)\,dt$$
$$+ \sum_{i=1}^{N_x} \int_0^T \sum_{k=1}^{N_x} y_k^T(t)F_{k,i}(S(t))x_i'(t)\,dt$$
$$+ \sum_{j=1}^{N_\alpha} \int_0^T \sum_{k=1}^{N_x} y_k^T(t)G_{k,j}(S(t))\,dt\,\alpha_j'$$
$$\sum_{k=1}^{N_x} y_k^T(T)x_k'(T) = \sum_{i=1}^{N_x} \int_0^T (\dot{y}_i(t) +$$
$$+ \sum_{k=1}^{N_x} F_{k,i}^T(S(t))y_k)^T x_i'(t)\,dt$$
$$+ \sum_{j=1}^{N_\alpha} \left(\int_0^T \sum_{k=1}^{N_x} G_{k,j}^T(S(t))y_k(t)\,dt \right)\alpha_j'.$$

And, by choosing

$$\dot{y}_i(t) = -\sum_{k=1}^{N_x} F_{k,i}^T(S(t))y_k(t)$$
$$y_i(T) = \bar{x}(T) - \bar{x}(0),$$

and using equation (11), this gives

$$J'(\alpha) = \frac{1}{N_x T^2} \sum_{j=1}^{N_\alpha} \left(\int_0^T \sum_{k=1}^{N_x} G_{k,j}^T(S(t))y_k(t)\,dt \right)\alpha_j'.$$

By defining $z_k(t) \triangleq y_k(T-t)$, $\bar{F}_{k,i}(t) \triangleq F_{k,i}^T(S(T-t))$, and $\bar{G}_{k,j}(t) \triangleq G_{k,j}^T(S(T-t))$, then

$$\dot{z}_i(t) = \sum_{k=1}^{N_x} \bar{F}_{k,i}(t)z_k(t)$$
$$z_i(0) = \bar{x}(T) - \bar{x}(0), \qquad (12)$$

and

$$J'(\alpha) = \frac{1}{N_x T^2} \sum_{j=1}^{N_\alpha} \left(\int_0^T \sum_{k=1}^{N_x} \bar{G}_{k,j}(t)z_k(t)\,dt \right)\alpha_j'.$$

Hence, it is possible to identify the gradient of the cost functional as:

$$\frac{\partial J}{\partial \alpha_j}(\alpha) = \frac{1}{N_x T^2} \int_0^T \sum_{k=1}^{N_x} \bar{G}_{k,j}(t)z_k(t)\,dt. \qquad (13)$$

This result can now be used in any gradient ascent algorithm (as it is also illustrated in [9], [15], [16]) to maximize the desired functional. In order to keep the design parameter α with positive components (since negative elasticity does not make physical sense), we will also add a barrier term to our functional:

$$B = \frac{\lambda}{N_\alpha} \sum_{j=1}^{N_\alpha} \log(\alpha_j), \qquad (14)$$

where λ is a fixed constant.

D. Optimization Results

As described in section II-B, the flagellum is discretized using triangular cross sections perpendicular to the helix centerline of the structure. The spring connections defined can be categorized into 4 types (see figure 4): cross sectional (between particles in the same cross-section), longitudinal (between corresponding particles in the following cross-section), diagonal and anti-diagonal (between any other particles in the following cross-section that has not been connected yet). We distinguish between three components in each category due to triangular cross sections in our model.

For the optimization process, each of these types of spring connections is initialized to the same constant elasticity value. The gradient is computed by using equations (12)-(13), and then used to update the elasticity coefficients by gradient ascent. The optimal distribution yields a 76% increase of the mean forward speed over the initial uniform distribution.

Figure 6 shows the elasticity distribution for the different components along the flagellum after convergence of the algorithm. We observe a large increase on the longitudinal coefficients, while a decrease along the diagonals. Since the longitudinal springs have the effect of mantaining the length of the flagellum constant, and the diagonals can be associated to the torsion of the flagellum, then the optimal distribution allows for more torsion on the structure while enforcing a constant length. We also note that there is little variation on the cross-sectional coefficents and torward the end of the flagellum.
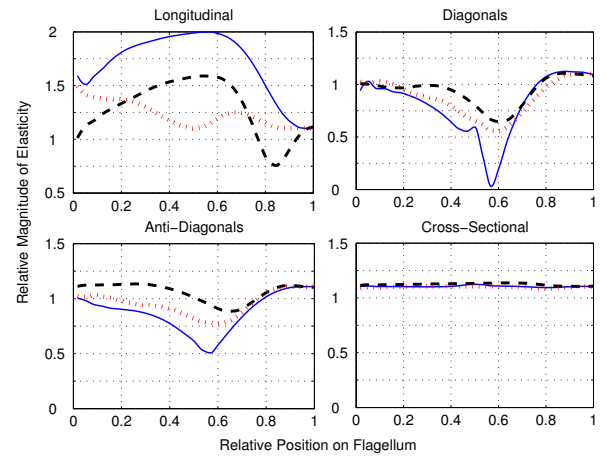

Fig. 6. Plots of the elasticity components along the flagellum. The x-axis depicts the relative position along the arc-length of the flagellum where 0 is at the base and 1 is at the end. The y-axis is the magnitude of the gradient component relative to the initial uniform distribution. Due to triangular cross sections, there are three components for each gradient category. This components are illustrated in figure 4.

Since the optimization involves the motion of the average particle, it is useful to analyze the trajectory traced by it. In figure 7 we observe two trajetories on the xy-plane. On the top, it is observed the trajectory for the initial uniform distribution (before any gradient updates). On the bottom, the trajectory for the optimal distribution is shown. It is observed
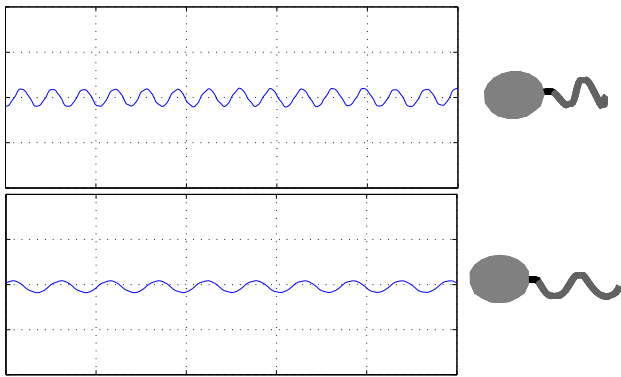
Fig. 7. Trajectories on the xy plane of the average particle before optimization (top-left) and after (bottom-left), and their corresponding (not at scale) motion configurations (right).

that there is no noticeable change on the frequency of rotation on these helical paths. Some statistics comparing these two paths are shown in table I.

TABLE I
STATISTISTIC ON PATH FOR MEAN PARTICLE AFTER OPTIMIZATION

	Relative change from Initial
Mean Forward Speed	+ 76 %
Frequency of Oscillation	+ 12 %
Amplitude of Oscillation	− 31 %

There is also a noticeable difference between the configurations of the bacterial structure during motion. On the top-right of figure 7, the plot shows a configuration of the structure during motion before any gradient update is applied. On the bottom-right of the same figure, a configuration during motion after optimization is shown. There is a noticeable increase on the pitch of the helical structure.

IV. CONCLUSIONS AND FUTURE WORK

The motion modeling section successfully simulates bacterial forward motion and change of orientation by reversing the torque for a single-flagellum organism. For the optimization part of this paper, the aim was to maximize the forward speed in terms of the elasticity distribution on the flagellum. By use of the adjoint method, it was shown how to come up with an appropriate estimate for the gradient of the forward speed. This estimate of the gradient was also successfully used for computing elasticity distributions that a yield higher speed. This analysis can easily be extended to optimizing structural shape of the flagellum.

The model can be improved by including other boundary conditions that are more suitable such as planes with no-slip boundary conditions, in which case this simulations can be directly compared to experimental results such as the ones presented by B. Behkam et al. [8]. There is also the possibility of including control mechanisms for trajectory tracking in this model. This could be particularly interesting for the design of nanobots.

REFERENCES

[1] J. P. Armitage and R. Schmitt, "Bacterial chemotaxis: Rhodobacter sphaeroides and sinorhizobium meliloti - variations on a theme?" *Microbiology*, vol. 143, pp. 3671–3682, 1997.
[2] J. P. Armitage, T. P. Pitta, M. A. Vigeant, H. L. Packer, and R. M. Ford, "Transformations in flagellar structure of rhodobacter sphaeroides and possible relationship to changes in swimming speed," *Journal of Bacteriology*, vol. 181(16), pp. 4825–4833, 1999.
[3] E. M. Purcell, "The efficiency of propulsion by a rotating flagellum," *Proc. Natl. Acad. Sci. USA*, vol. 94, pp. 11 307–11 311, 1997.
[4] H. Flores, E. Lobaton, S. Mendez-Diez, S. Tluvapova, and R. Cortez, "A study of bacterial flagellar bundling," *Bulletin of Mathematical Biology*, vol. 67, pp. 137–168, 2005.
[5] A. Najafi and R. Golestanian, "Simple swimmer at low reynolds number: three linked spheres," *Physical Review E*, vol. 69, pp. 062 901–062 904, 2004.
[6] R. Dreyfus, J. Baudry, M. L. Roper, M. Fermigier, H. A. Stone, and J. Bibette, "Microscopic artificial swimmers," *Nature*, vol. 437(6), pp. 862–865, 2005.
[7] J. J. H. Long, A. C. Lammert, C. A. Pell, M. Kemp, J. A. Strother, H. C. Cheenshaw, and M. J. McHenry, "A navigational primitive: Biorobotic implementation of cycloptic helical klinotaxis in planar motion," *IEEE Journal of Oceanic Engineering*, vol. 29, pp. 795–806, 2004.
[8] B. Behkam and M. Sitti, "Design methodology for biomimetic propulsion of miniature swimming robots," *ASME Journal of Dynamic Systems, Measurement, and Control*, vol. 128(1), pp. 36–43, 2006.
[9] R. L. Raffard, K. Amonlirdviman, J. D. Axelrod, and C. J. Tomlin, "Automatic parameter identification via the adjoint method, with application to understanding planar cell polarity," in *Proceedings of the 45th IEEE Conference on Decision and Control*, San Diego, CA, Dec. 2006.
[10] K. Amonlirdviman, N. A. Khare, D. R. P. Tree, W. S. Chen, J. D. Axelrod, and C. J. Tomlin, "Mathematical modeling of planar cell polarity to understand domineering nonautonomy," *Science*, vol. 307, no. 3, pp. 423–426, 2005.
[11] A. Jameson, "Aerodynamic design via control theory," *Journal of Scientific Computing*, vol. 3, no. 3, pp. 233–260, 1988.
[12] T. R. Bewley, "Flow control: New challenges for a new renaissance," *Progress in Aerospace Sciences*, vol. 37, pp. 21–58, 2001.
[13] O. M. Aamo and M. Krstic, *Flow Control by Feedback*. Springer-Verlag, 2002.
[14] D. Jacquet, M. Krstic, and C. C. de Wit, "Optimal control of scalar one-dimensional conservation laws," in *Proceedings of the 2005 American Control Conference*, Minneapolis, MN, June 2006, pp. 2499–2504.
[15] A. M. Bayen, R. Raffard, and C. J. Tomlin, "Adjoint-based control of a new eulerian network model of air traffic flow," *IEEE Transactions on Control Systems Technology*, vol. 14, no. 5, pp. 804–818, 2006.
[16] I. Strub and A. M. Bayen, "Optimal control of air traffic networks using continuous flow models," in *AIAA Paper 2006-0228, AIAA Conference on Guidance, Control and Dynamics*, Keystone, CO, Aug. 2006.

APPENDIX I
COMPUTING $F_{k,i}$ AND $G_{k,j}$

By identifying the coefficient of α'_n in equation (9) to the coefficients in equation (10), it can be observed that

$$\sum_{n=1}^{N_\alpha} G_{k,n}(S(t))\alpha'_n = \sum_{j=1}^{N_x} D_3 U_s(x_k;x_j,f_j)\sum_{n=1}^{N_\alpha}(D_{\alpha_n}f_j)\alpha'_n$$

$$G_{k,n}(S(t)) = \sum_{j=1}^{N_x} D_3 U_s(x_k;x_j,f_j)\,D_{\alpha_n}f_j.$$

In the model, particles are joined by spring connections, and the total force applied at a particle location is the sum of the forces due to the springs connected to it, as seen in equation (5). Hence, $D_{\alpha_n} f_j$ is 0 if the n-th spring (with elasticity α_n) is not connected to x_j. Therefore, by defining $v(n)$ to be the set of particles connected by the spring with coefficient α_n, then we obtain

$$G_{k,n}(S(t)) = \sum_{j \in v(n)} D_3 U_s(x_k; x_j, f_j) D_{\alpha_n} f_j. \quad (15)$$

By identification of the coefficients of x_i' between equations (9) and (10), it can be concluded that

$$\begin{aligned}
\sum_{n=1}^{N_x} F_{k,n}(S(t)) x_n' = \sum_{i=0}^{3} & [D_1 U_r(x_k; x_{n_i}, L_i) x_k' \\
& + D_2 U_r(x_k; x_{n_i}, L_i) x_{n_i}' \\
& + D_3 U_r(x_k; x_{n_i}, L_i) \sum_{m \in B} (D_{x_m} L_i) x_m'] \\
+ \sum_{j=1}^{N_x} & [D_1 U_s(x_k; x_j, f_j) x_k' + D_2 U_s(x_k; x_j, f_j) x_j' \\
& + D_3 U_s(x_k; x_j, f_j) \sum_{m=1}^{N_x} (D_{x_m} f_j) x_m']
\end{aligned}$$

Then,

$$\begin{aligned}
F_{k,n}(S(t)) = \sum_{i=0}^{3} & D_1 U_r(x_k; x_{n_i}, L_i)[\text{If } k = n] \\
& + D_2 U_r(x_k; x_n, L_n)[\text{If } n \in R] \\
& + \sum_{i=0}^{3} D_3 U_r(x_k; x_{n_i}, L_i) D_{x_n} L_i[\text{If } n \in R] \\
& + \sum_{j=1}^{N_x} D_1 U_s(x_k; x_j, f_j)[\text{If } k = n] \\
& + D_2 U_s(x_k; x_n, f_n) \\
& + \sum_{j \in c(n)} D_3 U_s(x_k; x_j, f_j) D_{x_n} f_j \\
& + D_3 U_s(x_k; x_n, f_n) D_{x_n} f_n,
\end{aligned}$$

$$(16)$$

where $c(n)$ is the set of particles connected to x_n by some spring. For the last two term we used the fact that $D_{x_n} f_j$ is nonzero only for those forces for which x_n is part of the computation, i.e. the set $c(n) \cup \{x_n\}$.

APPENDIX II
LIST OF DERIVATIVES OF FUNCTIONS

All the derivatives required for the above computations are defined in this Appendix.

A. Derivatives of rotlet component

The expression for the velocity contribution from the rotlet solutions is given in equation (3) by

$$U_r(x_k; x_{n_i}, L_i) = \frac{(2 r_{k n_i}^2 + 5 \delta^2)}{16 \pi (r_{k n_i}^2 + \delta^2)^{5/2}} [L_i \times (x_k - x_{n_i})],$$

where $r_{k n_i}$ is the euclidean distance between x_k and x_{n_i}, and δ is the regularization parameter.

Hence,

$$\begin{aligned}
D_1 U_r(x_k; x_{n_i}, L_i) = & -\frac{(6 r_{k n_i}^2 + 21 \delta^2)}{16 \pi (r_{k n_i}^2 + \delta^2)^{7/2}} [L_i \times (x_k - x_{n_i})] \\
& \cdot (x_k - x_{n_i})^T + \frac{(2 r_{k n_i}^2 + 5 \delta^2)}{16 \pi (r_{k n_i}^2 + \delta^2)^{5/2}} \widehat{L_i},
\end{aligned}$$

where $\widehat{L_i}$ is the skew symmetric operator $\widehat{}$ applied to the vector L_i. Also,

$$D_2 U_r(x_k; x_{n_i}, L_i) = -D_1 U_r(x_k, x_{n_i}, L_i).$$

And,

$$D_3 U_r(x_k; x_{n_i}, L_i) = -\frac{(2 r_{k n_i}^2 + 5 \delta^2)}{16 \pi (r_{k n_i}^2 + \delta^2)^{5/2}} (\widehat{x_k - x_{n_i}}).$$

B. Derivatives of Stokeslet component

The expression for the velocity contribution from the rotlet solutions is given in equation (2) by

$$U_s(x_k; x_i, f_i) = \frac{(r_{k i}^2 + 2 \delta^2)}{8 \pi (r_{k i}^2 + \delta^2)^{3/2}} f_i + \frac{[f_i^T (x_k - x_i)]}{8 \pi (r_{k i}^2 + \delta^2)^{3/2}} (x_k - x_i).$$

Hence,

$$\begin{aligned}
D_1 U_s(x_k; x_i, f_i) = & -\frac{(r_{k i}^2 + 4 \delta^2)}{8 \pi (r_{k i}^2 + \delta^2)^{5/2}} f_i (x_k - x_i)^T \\
& + \frac{1}{8 \pi (r_{k i}^2 + \delta^2)^{3/2}} (x_k - x_i) f_i^T \\
& - \frac{3 [f_i^T (x_k - x_i)]}{8 \pi (r_{k i}^2 + \delta^2)^{5/2}} (x_k - x_i)(x_k - x_i)^T \\
& + \frac{[f_i^T (x_k - x_i)]}{8 \pi (r_{k i}^2 + \delta^2)^{3/2}} I.
\end{aligned}$$

Also,

$$D_2 U_s(x_k; x_i, f_i) = -D_1 U_s(x_k, x_i, f_i).$$

And,

$$\begin{aligned}
D_3 U_s(x_k; x_i, f_i) = & \frac{(r_{k i}^2 + 2 \delta^2)}{8 \pi (r_{k i}^2 + \delta^2)^{3/2}} I \\
& + \frac{1}{8 \pi (r_{k i}^2 + \delta^2)^{3/2}} (x_k - x_i)(x_k - x_i)^T.
\end{aligned}$$

C. Derivatives of the torques

The torques, as given in equation (6), are defined as

$$L_i = \sigma_i \frac{p}{||p||},$$

where $p \triangleq (x_{n_0} - (x_{n_1} + x_{n_2} + x_{n_3})/3)$, σ_i is the magnitude of the torque, $n_j \in R$ are the indexes of the points used for computing the direction of the torque and where the torques are applied.

Clearly, if $k \notin R$ then $D_{x_k} L_i = 0$. In the case that $k = n_0$, then

$$D_{x_{n_0}} L_i = \frac{\sigma_i}{||p||} I - \frac{\sigma_i}{||p||^3} p\, p^T.$$

Also,

$$D_{x_{n_1}} L_i = D_{x_{n_2}} L_i = D_{x_{n_3}} L_i = -\frac{1}{3} D_{x_{n_0}} L_i.$$

D. Derivatives of the forces

The forces are also defined in equation (5) as

$$f_i = \sum_{n \in c(i)} \alpha_{in} \left(1 - \frac{r_{0,in}}{r_{in}}\right) (x_n - x_i)$$

where α_{in} is the elasticity constant between x_n and x_i, and $r_{0,in}$ is the rest length between x_n and x_i.

Clearly, if $k \notin c(i)$ and $k \neq i$ then $D_{x_k} f_i = 0$. Otherwise, for $k \in c(i)$

$$\begin{aligned}
D_{x_k} f_i = & \alpha_{ik} \left(\frac{r_{0,ik}}{r_{ik}^3}\right) (x_k - x_i)(x_k - x_i)^T \\
& + \alpha_{ik} \left(1 - \frac{r_{0,ik}}{r_{ik}}\right) I.
\end{aligned}$$

And,

$$D_{x_i} f_i = -\sum_{k \in c(i)} D_{x_k} f_i$$

We also have that

$$D_{\alpha_{in}} f_i = \left(1 - \frac{r_{0,in}}{r_{in}}\right) (x_n - x_i),$$

for α_{in} connecting x_n to x_i. In general, if α_k does not connect any node to x_i, then $D_{\alpha_k} f_i = 0$.